

Statistical Analysis for Satellite Index-Based Insurance to define Damaged Pasture Thresholds

Juan José Martín-Sotoca^{1*}, Antonio Saa-Requejo^{2,3}, Rubén Moratíel^{2,3}, Nicolas Dalezios⁴, Ioannis Faraslis⁵, and Ana María Tarquis^{2,6}

jmartinsotoca@gmail.com, antonio.saa@upm.es, ruben.moratíel@upm.es, dalezios.n.r@gmail.com, faraslisgiannis@yahoo.gr, anamaria.tarquis@upm.es

¹ Data Science Laboratory. European University, Madrid, Spain.

² CEIGRAM, Research Centre for the Management of Agricultural and Environmental Risks, Madrid, Spain.

³ Dpto. Producción Agraria. Universidad Politécnica de Madrid, Spain.

⁴ Department of Civil Engineering. University of Thessaly, Volos, Greece.

⁵ Department of Planning and Regional Development. University of Thessaly, Volos, Greece.

⁶ Grupo de Sistemas Complejos. Universidad Politécnica de Madrid, Spain.

* Correspondence to: jmartinsotoca@gmail.com

Abstract: Vegetation indices based on satellite images, such as Normalized Difference Vegetation Index (NDVI), have been used in countries like USA, Canada and Spain for damaged pasture and forage insurance for the last years. This type of agricultural insurance is called “satellite index-based insurance” (SIBI). In SIBI, the occurrence of damage is defined through NDVI thresholds mainly based on statistics derived from Normal distributions. In this work a pasture area at the north of Community of Madrid (Spain) has been delimited by means of Moderate Resolution Imaging Spectroradiometer (MODIS) images. A statistical analysis of NDVI histograms was applied to seek for alternative distributions using maximum likelihood method and χ^2 test. The results show that the Normal distribution is not the optimal representation and the General Extreme Value (GEV) distribution presents a better fit through the year based on a quality estimator. A comparison between Normal and GEV are showed respect to the probability under a NDVI threshold value along the year. This suggests that a priori distribution should not be selected and a percentile methodology should be used to define a NDVI damage threshold rather than the average and standard deviation, typically of Normal distributions.

Keywords: NDVI, pasture insurance, GEV distribution, MODIS.

Highlights

- The GEV distribution provides better fit to the NDVI historical observations than the Normal one.
- Difference between Normal and GEV distributions are higher during spring and autumn, transition periods in the precipitation regimen.
- NDVI damage threshold shows evident differences using Normal and GEV distributions covering both the same probability (24.20%).
- NDVI damage threshold values based on percentiles calculation is proposed as an improvement in the index based insurance in damaged pasture.

42

43 **1. Introduction**

44 Agricultural insurance addresses the reduction of the risk associated with crop
45 production and animal husbandry. The concept of index-based insurance (IBI) attempts
46 to achieve settlements based on the value taken by an objective index rather than on a
47 case-by-case assessment of crop or livestock losses (Gommes and Kayitakier, 2013).
48 Indeed, the goal of IBI policy remains to develop an affordable tool to all producers,
49 including smallholders. Specifically, IBI can constitute a safety net against
50 weather-related risks for all members of the farming community, thereby increasing
51 food security and reducing the vulnerability of rural populations to weather extremes.
52 Moreover, IBI can be associated with credits for insured smallholders, due to the fact
53 that the risk of non-repayment for lenders is reduced, which encourages the use of
54 agricultural inputs and equipment, leading to increased and more stable crop
55 production. Over the past decade, the importance of weather index-based insurances
56 (WIBI) for agriculture has been increasing, mainly in developing countries (Gommes
57 and Kayitakier, 2013). This interest can be explained by the potential that IBI
58 constitutes a risk management instrument for small farmers. Indeed, it can be
59 considered within the context of renewed attention to agricultural development as
60 one of the milestones of poverty reduction and increased food security, as well as the
61 accompanying efforts from various stakeholders to develop agricultural risk
62 management instruments, including agricultural insurance products.

63

64 Farmers need to protect their land and crops specifically from drought in arid and
65 semi-arid countries, since their production may directly depend mainly on the impacts
66 of this particular natural hazard. Insurance for drought-damaged lands and crops is
67 currently the main instrument and tool that farmers can resort in order to deal with
68 agricultural production losses due to drought. Many of these insurances are using
69 satellite vegetation indices (Rao, 2010), thus they are also called “satellite index-based
70 insurances” (SIBI). SIBI have some advantages over WIBI, such as cost-effective
71 information and acceptable spatial and temporal resolution. They do not, however,
72 resolve the issue of basis risk, i.e. potential unfairness to insurance takers (Leblois,
73 2012). Moreover, the very nature of an index-based product creates the chance that
74 an insured party may not be paid when they suffer loss. For this reason, in some
75 countries (Spain) they have named this SIBI as “damaged in pasture” to cover not only
76 drought even this one is the main cause.

77

78 It is highly recognized that shortage of water has many implications to agriculture,
79 society, economy and ecosystems. Specifically, its impact on water supply, crop
80 production and rearing of livestock is substantial in agriculture. Knowing the likelihood
81 of drought is essential for impact prevention (Dalezios, 2013). Drought severity

82 assessment can be approached in different ways: through conventional indices based
 83 on meteorological data, such as temperature, rainfall, moisture, etc. (Niemeyer, 2008),
 84 as well as through remote sensing indices based on images usually taken by artificial
 85 satellites (Lovejoy et al., 2008) or drones. In the second group they are found Satellite
 86 Vegetation Indices (SVI), which can quantify “green vegetation”, and soil moisture
 87 through Soil Water Index (Gouveia et al., 2009) combining different spectral
 88 reflectances. Thus, they are one of the main ways to quantitatively assess drought
 89 severity.

90

91 At the present time, several satellites (NOAA, TERRA, DEIMOS, etc.) can provide
 92 this spectral information with different spatial resolution. Some series with a high
 93 temporal frequency are freely available, those from NOAA satellites and Terra. The
 94 most widely known SVI is the Normalized Difference Vegetation Index (NDVI). It
 95 follows the principle that healthy vegetation mainly reflects the near-infrared
 96 frequency band. There are several other important SVI, such as Soil Adjusted
 97 Vegetation Index (SAVI) and Enhanced Vegetation Index (EVI) that incorporate soil
 98 effects and atmospheric impacts, respectively. An important point of SIBI is “when
 99 damage occurs”. To measure this, a SVI threshold value is defined mainly based on
 100 statistics that apply to Normal distributed variables: average and standard deviation.
 101 When current SVI values are bellow this threshold value for a period of time, insurance
 102 recognizes that a damage is occurring, most of the times drought, and then it begins to
 103 pay compensations to farmers.

104

105 Important NDVI-based indices for detecting drought are NDVI anomalies (NDVIA)
 106 and Standardized Vegetation Index (SVI). NDVIA and SVI have been successfully used
 107 to monitor drought conditions over different regions in the world (Nanzad et al., 2019;
 108 Li et al., 2014). NDVIA is calculated as the difference between the NDVI value for a
 109 specific time period (e.g., week, month) and the long-term mean value for that period.
 110 SVI was developed by Peters et al. (2002) and obtains the probability from normal
 111 NDVI distributions over multiple years of data, on a time period (Anyamba and Tucker,
 112 2012; Bayarjargal et al., 2006). It is defined as:

113

$$114 \quad SVI_i = \frac{NDVI_i - \overline{NDVI}}{\sigma_{NDVI}} = \frac{NDVIA_i}{\sigma_{NDVI}} \quad (1)$$

115

116 where \overline{NDVI} is the long-term mean NDVI in the period i , σ_{NDVI} is the standard
 117 deviation of NDVI in the period i , and $NDVI_i$ is the current NDVI value in the time
 118 period i . Using only the first and second statistical moment, average and the square
 119 root of variance, the assumption of normality is implicit in this type of drought NDVI
 120 indicator. The normality assumption is challenged in this study.

121

122 WIBI aims to protect farmers against weather-based disasters such as droughts,
123 frosts and floods. A WIBI policy links possible insurance payouts with the weather
124 requirements of the crop being insured: the insurer pays an indemnity whenever the
125 realized value of the weather index meets a specified threshold. Whereas payouts in
126 traditional insurance programs are related to actual crop damages, a farmer insured
127 under a WIBI contract may receive a payout. A current difficulty to the wide
128 implementation of WIBI is the weakness of indices. Indeed, there is certainly a need for
129 more efficient indices based on the additional experience gained from the
130 implementation of WIBI products in the developing world. Current trends in index
131 technology are exciting and they actuate high expectations, especially the
132 development of yield indices and the use of remote sensing inputs. Risk protection and
133 insurance illiteracy constitute another difficulty, which has to be addressed by training
134 and awareness-raising at all levels, from farmers to farmers' associations,
135 micro-insurance partners, as well as senior decision-makers in insurance, banking, and
136 politics (Bailey, 2013). It is essential that all stakeholders (especially the insured)
137 perfectly understand the principles of IBI, as otherwise the insurer, even the whole
138 concept of insurance, is at risk of reputation loss for years or decades.

139
140 There is currently a lack of technical capacity in the insurance sectors of most
141 developing countries, which is a constraint to the scaling up and further development
142 of WIBI (Gommes and Kayitakire, 2012). Specifically, although it is possible to design an
143 index product and assist in roll-out, marketing, and sales, such assistance is not
144 possible on a wide scale, simply because there is lack of qualified expertise. Indeed, it
145 usually requires mathematical modeling, data manipulation, and expertise in crop
146 simulation to design an index. Nevertheless, it is possible to structure insurance with
147 multiple indices, but this increases the complexity of the product and makes it difficult
148 for farmers to comprehend it. 'Basis risk' is also a particular problem for index
149 products, which is frequently caused by the fact that measurements of a particular
150 variable, such as rain, may differ at the insurer's measurement site and in the farmer's
151 field. This also creates problems for insurance providers. Indeed, part of the reason the
152 scaling up of index products has failed is that both insurers and farmers suffer from
153 this basis risk.

154
155 Currently, to mitigate impacts of climate-related reduced productivity of French
156 grasslands, several studies have been developed to design new insurance scheme
157 bases indemnity payouts to farmers on a forage production index (FPI) (Rumiguié et
158 al., 2015; 2017). Two examples of SIBIs are presented in two different countries: USA
159 and Spain. In particular, in USA there are several insurance programs for pasture,
160 rangeland and forage, which use various indexing systems (rainfall and vegetation
161 indices), and are promoted by Unites States Department of Agriculture (USDA) (Maples
162 et al., 2016; USDA, 2018). NDVI is the index chosen in the vegetation index program

163 and it is obtained from AVHRR (Advanced Very High Resolution Radiometer) sensor
 164 onboard NOAA satellites. Average, maximum and minimum NDVI values are obtained
 165 from a historical series with the aim of calculating a trigger value. Insurer decides the
 166 quantity of compensation comparing this trigger with current value. On the other
 167 hand, in Spain there exists the “Insurance for Damaged Pasture” from “Spanish System
 168 of Agricultural Insurance” (BOE, 2013). This insurance defines damage event through
 169 NDVI values obtained from MODIS sensor onboard TERRA satellite of NASA. In this
 170 insurance, NDVI threshold values ($NDVI_{th}$) are calculated subtracting several times
 171 ($k = 0.7$ or $k = 1.5$) standard deviation to average within a homogeneous area:

172

$$173 \quad NDVI_{th} = \mu - k \cdot \sigma \quad (2)$$

174

175 where μ, σ are average and standard deviation of NDVI respectively. Average and
 176 standard deviation come of supposing Normal distributions in the historical data
 177 (Goward et al., 1985; Hobbs, 1995; Fuller, 1998; Al-Bakri and Taylor, 2003; Turvey et
 178 al., 2012; De Leeuw et al. 2014).

179

180 The aim of this paper is to find a more realistic statistical NDVI distribution without
 181 the “a priori” assumption that variables follow a Normal distribution, typically for
 182 current SIBI methodology. In order to achieve this, the Maximum Likelihood Method
 183 (MLM) is fitted to a historical series of NDVI values in a pasture land area in Spain
 184 (Community of Madrid). Different types of asymmetrical distributions are examined
 185 with the aim to find a better fit than Normal. To eliminate some noise in the historical
 186 series, an original method is applied consisting of using Hue-Saturation-Lightness (HSL)
 187 color model. Finally, Chi-square test (χ^2 test) has been used to check the goodness of
 188 fit for all considered distributions.

189

190

191 **2. Materials and Methods**

192 **2.1 Vegetation Index**

193 The differences of the reflectance of green vegetation in parts of the
 194 electromagnetic radiation spectrum, namely, visible and near infrared, provide an
 195 innovative method for monitoring surface vegetation from space. Specifically, the
 196 spectral behavior of vegetation cover in the visible (0.4-0.7mm) and near infrared
 197 (0.74-1.1mm, 1.3-2.5mm) offers the possibility to monitor from space the changes in
 198 the different stages of cultivated and uncultivated plants taking also into account the
 199 corresponding behavior of the surrounding microenvironment (Ortega-Farias et al.,
 200 2016). Indeed, from the visible part of the electromagnetic radiation spectrum it is
 201 possible to draw conclusions about the rate photosynthesis, whereas from near

202 infrared inferences are extracted about the chlorophyll density and the amount of
 203 canopy in the plant mass, as well as the water content in the leaves, which is also
 204 linked directly to the rate of transpiration with impacts to physiological process of
 205 photosynthesis. Usually, data from NOAA/AVHRR series of polar orbit meteorological
 206 satellites are used with low spatial resolution (1.1 km²) and recurrence interval at least
 207 twice daily from the same location. Several algorithms combining channels of red
 208 (RED), near infrared (NIR) and green (GREEN) have been proposed, which provide
 209 indices sensitive to green vegetation.

210

211 NDVI uses two frequency bands: red band (660 nm) and near-infrared band (860
 212 nm). Absorption of red band is related to photosynthetic activity and reflectance of
 213 near-infrared band is related to presence of vegetation canopies (Flynn, 2006). In
 214 drought periods, NDVI values can reduce significantly, therefore many researchers
 215 have used this index to measure drought events in recent years (Dalezios et al., 2014).
 216 To calculate NDVI we will use this mathematical formula:

217

$$218 \quad NDVI = \frac{IR-R}{IR+R} \quad (3)$$

219

220 where “IR” and “R” are reflectance values in Near-Infrared band and Red band,
 221 respectively. NDVI values below zero indicate no photosynthetic activity and are
 222 characteristic of areas with large accumulation of water, such as rivers, lakes, or
 223 reservoirs. The higher is the NDVI value, the greater is the photosynthetic activity and
 224 vegetation canopies.

225

226 In this paper, the NDVI is used, which is widely known index with a multitude of
 227 applications over time. The NDVI is suited for monitoring of total vegetation, since it
 228 partly compensates the changes in light conditions, land slope and field of view (Kundu
 229 et al., 2016). In addition, clouds, water and snow show higher reflectance in the visible
 230 than in the near infrared, thus, they have negative NDVI values. Indeed, bare and rocky
 231 terrain show vegetation index values close to zero. Moreover, the NDVI constitutes a
 232 measure of the degree of absorption by chlorophyll in the red band of the
 233 electromagnetic spectrum. In summary, the NDVI is a reliable index of the chlorophyll
 234 density on the leaves, as well as the percentage of the leaf area density over land,
 235 thus, NDVI constitutes a credible measure for the assessment of dry matter (biomass)
 236 in various species vegetation cover (Dalezios, 2013). It is clear from the above that the
 237 NDVI is an index closely related to growth and development of plants, which can
 238 effectively monitor surface vegetation from space.

239

240 The continuous increase of the NDVI value during the growing season reflects the
 241 vegetative and reproductive growth due to intense photosynthetic activity, as well as

242 the satisfactory correlation with the final biomass production at the end of a growing
243 period. On the other hand, gradual decrease of the NDVI values signifies stress due to
244 lack of water or extremely high temperatures for the plants, leading to a reduction of
245 the photosynthetic rate and ultimately a qualitative and quantitative degradation of
246 plants. NDVI values above zero indicate the existence of green vegetation
247 (chlorophyll), or bare soil (values around zero), whereas values below zero indicate the
248 existence of water, snow, ice and clouds.
249

250 **2.2 Database**

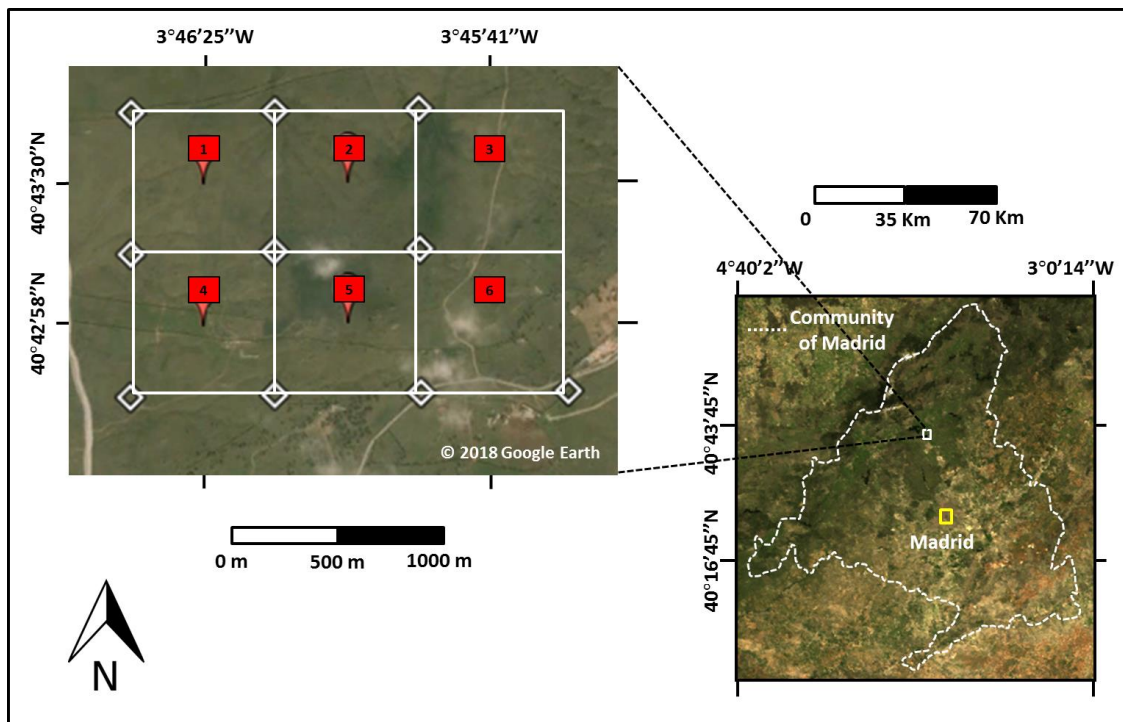
251 Scientific research satellite Terra (EOS AM-1) has been chosen to provide
252 necessary information to calculate NDVI in the study area. This satellite was launched
253 into orbit by NASA on December 18, 1999. MODIS sensor aboard this satellite collects
254 information of different reflectance bands. MODIS information is organized by
255 "products". The product used in this study was MOD09A1 (LP DAAC, 2014). MOD09A1
256 incorporates seven frequency bands: Band 1 (620-670 nm), band 2 (841-876 nm), band
257 3 (459-479 nm), band 4 (545-565 nm), 5 band (1230-1250 nm), band 6 (1628-1652 nm)
258 and band 7 (2105-2155 nm). The bands used to calculate NDVI are: band 1 for red
259 frequency and band 2 for near-infrared frequency. MOD09A1 provides georeferenced
260 images with pixel resolution of 500m x 500m. Each MOD09A1 pixel contains the best
261 possible L2G observation during an 8-day period as selected on the basis of high
262 observation coverage, low view angle, the absence of clouds or cloud shadow, and
263 aerosol loading.
264

265 The period of time selected on this study was from 2002 to 2017.
266

267 Daily data from a principal station of the meteorological network were utilized
268 during the period studied (2002 – 2017). Meteorological station is located in
269 40°41'46"N 3°45'54"W (elevation 1004 m a.s.l.), less than 2 km from the study area
270 (AEMET, 2017).
271

272 **2.3 Site description**

273 Six pixels (500m x 500m) are considered located in a pasture area at the north of
274 the Community of Madrid (Spain) between the municipalities of "Soto del Real" and
275 "Colmenar Viejo". The study area is located between meridians 3° 45' 00" and 3° 47'
276 00" W and parallels 40° 42' 00" and 40° 44' 00" N approximately (see Fig. 1).
277



278

279

280

Figure 1. The study area is in the centre of the Iberian Peninsula (Community of Madrid). RGB image of six pixels area used for case study is shown (Google Earth's and MODIS images).

281

282

283

284

285

286

287

288

289

The annual mean temperature ranges during the study period from 12.7°C to 13.8°C, and annual mean precipitation ranges from 360 mm to 781 mm. The stations studied were identified semi-arid (annual ratio P/ET_o between 0.2 and 0.5) according to the global aridity index developed by the United-Nations Convention to Combat Desertification (UNEP, 1997). According to the climatic classification of Köppen (Kottek et al., 2006), this area presents a continental Mediterranean climate temperate with dry and temperate summer (type Csb). Temperature and precipitation of this site, based on 20 years, is presented in Table 1.

290

291

292

293

294

Due to high soil moisture conditions, ash is the dominant tree, forming large agroforestry systems ("dehesas") that are used for pasture. These are ecosystems with high biodiversity.

295

296

Table 1. Monthly average of maximum temperature (T_{max}), average temperature (T_{avg}), minimum temperature (T_{min}) and precipitation (P). Study period from 1997 to 2017.

| Month | Jan | Feb | Mar | Apr | May | Jun | Jul | Aug | Sep | Oct | Nov | Dec | Annual |
|-----------------------|------|------|------|------|------|------|------|------|------|------|------|------|--------|
| T _{max} (°C) | 7.1 | 9.3 | 12.7 | 15.4 | 19.5 | 24.6 | 28.6 | 28.1 | 23.7 | 16.8 | 11.1 | 7.4 | 17.0 |
| T _{avg} (°C) | 3.6 | 4.8 | 7.7 | 10.1 | 13.7 | 18.4 | 22.0 | 21.7 | 17.9 | 12.3 | 7.1 | 4.1 | 12.0 |
| T _{min} (°C) | 0.0 | 0.3 | 2.6 | 4.8 | 7.8 | 12.1 | 15.4 | 15.3 | 12.0 | 7.8 | 3.0 | 0.8 | 6.8 |
| P (mm) | 67.2 | 50.0 | 38.5 | 62.2 | 62.3 | 30.2 | 18.9 | 16.4 | 34.2 | 79.3 | 86.2 | 82.6 | 627.9 |

297

298 **2.4 HSL model**

299 There is no doubt that NDVI time-series from satellite sensors carry useful
 300 information, which can be used for characterizing seasonal dynamics of vegetation
 301 (Fensholt et al., 2012; Forkel et al., 2013). However, due to unfavorable atmospheric
 302 conditions during the data acquisition, NDVI time-series curve often contains noise
 303 (Motohka et al., 2011; Park, 2013). Although most of the NDVI data products are
 304 temporally composited through maximum value compositing (MVC) method (Holben,
 305 1986) to retain relatively cloud-free data, residual noise still exists in the data, which
 306 will affect the accuracy of the NDVI value.

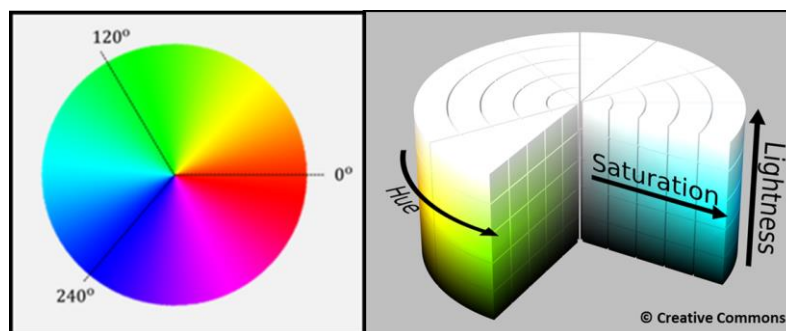
307

308 Therefore, usually it is necessary to reconstruct of NDVI time-series before
 309 extracting information from the noisy data. There are several techniques that have
 310 been applied to reduce noise and reconstruct NDVI series, a summary of these can be
 311 found in Wei et al. (2016). In this study we applied a simple filtering method based on
 312 the Hue-Saturation-Lightness (HSL) color model inspired by the work presented by
 313 Tackenberg (2007).

314

315 HSL color model is a cylindrical representation of RGB (Red-Green-Blue) points.
 316 Their components are Hue (color type), Saturation (level of color purity) and Lightness
 317 (color luminosity). Hue is the angular component and it is more intuitive for humans
 318 since it is directly related to the color wheel (see Fig. 2).

319



320

321 **Figure 2.** On the left: colour wheel of Hue. On the right: the HSL model (Creative Commons).

322

323 Saturation is the radial component and near-zero values indicate grey colors.
 324 Lightness is the axial radial versus axial component, zero lightness produces black and
 325 full lightness produces white.

326

327 The NDVI series are filtered using the following HSL criterion: NDVI values are valid
 328 if HSL Saturation is greater than 0.15. In this way, the values of the series that have

329 grey color correlate with pasture covered by clouds or snow are eliminated. This type
 330 of filter based in HSL color space has been used on digital camera images monitoring
 331 vegetation phenology (Tackenberg, 2007; Crimmins and Crimmins, 2008; Graham et
 332 al., 2009). However, we have not found the use of this HSL criterion in the context of
 333 NDVI remote sensing images.
 334

335 2.5 Maximum Likelihood Method

336 MLM estimates the set of parameters $\{\alpha, \beta, \mu, \sigma, \dots\}$ for a specific statistical
 337 distribution that maximizes the “likelihood function” or the “joint density function”:

$$338 \quad L = f(\mathbf{x}, \boldsymbol{\theta}) = \prod_{i=1}^n f(x_i; \alpha, \beta, \mu, \sigma, \dots) \quad (4)$$

339 where $\mathbf{x} = (x_1, \dots, x_n)$ is the set of data, $\boldsymbol{\theta} = (\alpha, \beta, \mu, \sigma, \dots)$ is the vector of
 340 parameters and $f(x_i; \alpha, \beta, \mu, \sigma, \dots)$ is the density function of the statistical model.

341 When maximization with respect to the vector of parameters is carried out, the
 342 estimated parameters $(\hat{\alpha}, \hat{\beta}, \hat{\mu}, \hat{\sigma}, \dots)$ for the proposed statistical distribution are
 343 obtained (Larson, 1982). Properties of estimated parameters are: invariance,
 344 consistency and asymptotically unbiased.

345 In the case of a Normal model, the estimated statistics μ and σ are defined by
 346 accurate expressions as follows:

$$347 \quad \hat{\mu} = \bar{x} = \frac{1}{n} \sum_{i=1}^n x_i \quad \hat{\sigma} = s = \sqrt{\frac{1}{n} \sum_{i=1}^n (x_i - \bar{x})^2} \quad (5)$$

348 where $\hat{\mu}$ is the sample mean and $\hat{\sigma}$ is the sample standard deviation of the data set.

349 In this study we will apply MLM to estimate the parameters for 4 probability
 350 density functions (PDF). In Table 2, a brief description is presented of these PDF
 351 candidates: Normal, Gamma, Beta and GEV. To do so, the following MATLAB functions
 352 have been used: “normfit”, “gamfit”, “betafit” and “gevfit” (respectively).
 353

354 **Table 2.** Candidate Probability Density Functions (PDF).

| PDF NAME | PDF EXPRESSION | PDF PARAMETERS |
|----------|--|---|
| Normal | $f(\mathbf{x}; \boldsymbol{\mu}, \boldsymbol{\sigma}) = \frac{1}{\sigma\sqrt{2\pi}} e^{-\frac{1}{2}\left(\frac{x-\mu}{\sigma}\right)^2}$ | $\boldsymbol{\mu} \equiv \textit{average}$ $\boldsymbol{\sigma} \equiv \textit{standard deviation}$ |
| Gamma | $f(\mathbf{x}; \boldsymbol{\alpha}, \boldsymbol{\beta}) = \frac{1}{\boldsymbol{\beta}^\alpha \Gamma(\boldsymbol{\alpha})} x^{\boldsymbol{\alpha}-1} e^{-\frac{x}{\boldsymbol{\beta}}}$ | $\Gamma(\cdot) \equiv \textit{gamma function}$ $\boldsymbol{\alpha}$ and $\boldsymbol{\beta} \equiv \textit{parameters}$ |
| Beta | $f(\mathbf{x}; \mathbf{a}, \mathbf{b}) = \frac{\Gamma(\mathbf{a} + \mathbf{b})}{\Gamma(\mathbf{a})\Gamma(\mathbf{b})} x^{\mathbf{a}-1} (1-x)^{\mathbf{b}-1}$ | $\Gamma(\cdot) \equiv \textit{gamma function}$ \mathbf{a} and $\mathbf{b} \equiv \textit{parameters}$ |

$$\begin{aligned}
 & f(x; \mu, \sigma, \xi) = \frac{1}{\sigma} t(x)^{\xi+1} e^{-t(x)} \\
 \text{GEV} \quad & \text{where } t(x) = \begin{cases} \left(1 + \left(\frac{x-\mu}{\sigma}\right)\xi\right)^{-1/\xi} & \text{if } \xi \neq 0 \\ e^{-(x-\mu)/\sigma} & \text{if } \xi = 0 \end{cases}
 \end{aligned}
 \quad \begin{array}{l}
 \mu \in \mathbb{R} \equiv \textit{location param.} \\
 \sigma > 0 \equiv \textit{scale parameter} \\
 \xi \in \mathbb{R} \equiv \textit{shape parameter}
 \end{array}$$

355

356

357 2.6 Goodness of fit (Chi square test)

358 χ^2 test can be used to determine to what extent observed frequencies differ from
 359 frequencies expected for a specific statistical model. The most important points of the
 360 theory are briefly presented in (Cochran, 1952).

361

362 Let $f(x, \theta)$ be a theoretical density function of a random variable X which
 363 depends on parameters $\theta = (\alpha, \beta, \mu, \sigma, \dots)$ and let x_1, \dots, x_n be a sample of X grouped
 364 into k classes with n_i data per class i .

365

366 Firstly, the following hypothesis is set:

367

368 (H_0) observed data fit theoretical distribution $f(x, \theta)$.

369 Then the test statistic χ_c^2 is defined as:

$$370 \quad \chi_c^2 = \sum_{i=0}^k \frac{(n_i - e_i)^2}{e_i} \quad (6)$$

371 where n_i is the number of data or observed frequency and $e_i = n \cdot P(\textit{class } i)$ is the
 372 expected frequency for class i . $P(\textit{class } i)$ is the theoretical interval probability
 373 defined for class i .

374 A level of significance is also set as:

$$375 \quad \alpha = P(\textit{Reject } H_0 / H_0 \textit{ is true}) \quad (7)$$

376 Finally, the following decision rule is applied: "reject the theoretical distribution at
 377 significance level α if:

$$378 \quad \chi_c^2 > \chi_{(k-m-1, 1-\alpha)}^2 \quad (8)$$

379 where $\chi_{(k-m-1, 1-\alpha)}^2$ is a χ^2 distribution with $k-m-1$ degrees of freedom (m is the
 380 number of parameters, k is the number of classes).

381

382

383

384

385 **3. Results**

386 **3.1 HSL filtering criterion**

387 NDVI series (from 2002 to 2017) were obtained for each pixel of the study area
388 using frequency bands provided by MODIS product named MOD09A1. These series
389 contain some irregular values that can skew NDVI pattern. Therefore, the six series (six
390 pixels) were filtered using the HSL criterion.

391

392 MOD09A1 is a MODIS product that processes data to obtain the best observation
393 in an 8-days period. However, it is possible that the result of this selection still presents
394 some problems since the best of this selection is relative to the eight observations of
395 the period. For example, if the eight observations, at one pixel, appear with clouds,
396 shadow clouds or snow, the best selection still shows this problem.

397

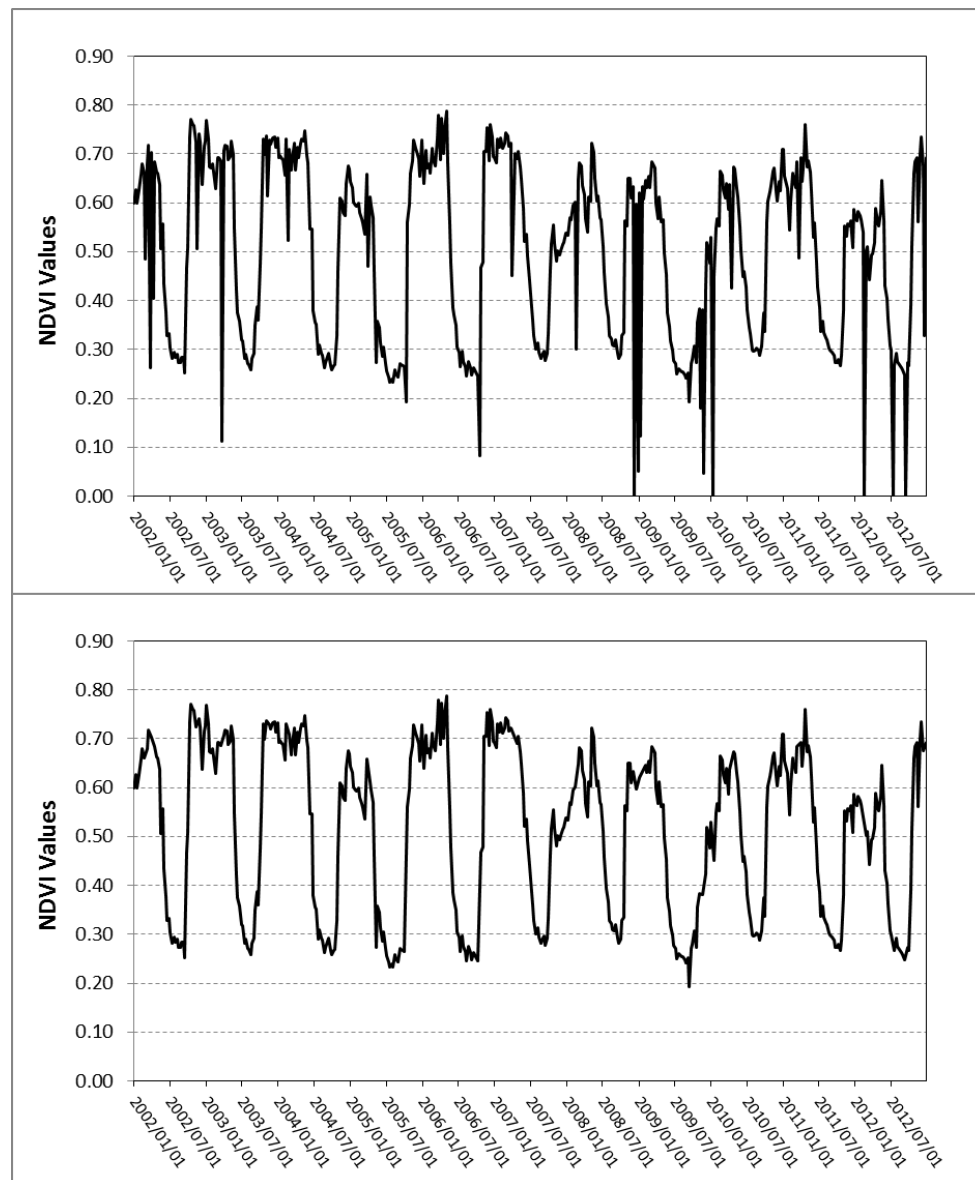
398 As an example of the above, the NDVI series (10 years) of one pixel of the study
399 area is shown in Fig. 3. On the top graph of Fig. 3 there are extremely low NDVI values
400 in some dates. If these NDVI values are compared to neighbouring values (8 days after
401 or before) the high variation presented in such short period is not plausible. This issue
402 tells us that the MODIS sensor has not obtained a proper observation during this 8
403 days period (interval).

404

405 The HSL criterion helps us to eliminate these incorrect NDVI values, since the filter
406 is interpreting that these pixels still contains clouds or snow, i.e., pixels with low
407 saturation (greyish colours).

408

409



410

411

412

Figure 3. HSL filtering criterion applied to a 10 years NDVI series. Top graph shows the real NDVI series. Bottom graph shows the HSL filtered NDVI series.

413

414

415

416

417

418

Fig. 3 shows that abrupt changes in the NDVI values, mainly observed during raining seasons such as autumn and winter, are efficiently eliminated. Not to be a high computational demanding method is one of the main advantages of HSL filtering method. Therefore, this method will allow us to obtain more robust NDVI values to be used in the statistical analysis.

419

3.2 Statistical analysis

420

421

422

423

NDVI values were obtained consecutively every 8 days from MODIS starting at the 1st of January of every year, in such a way that 46 NDVI observations were extracted for each year. Therefore, it was possible to define 46 Random Variables (RV) when all the years of this study were taking into account.

424 In Table 3, every RV (named as "Interval") is shown together with the number of
 425 available NDVI observations. Each RV collects the observations coming from the six
 426 selected pixels; therefore the maximum number of observations per RV could be: 6
 427 pixels x 16 years = 96 observations. The start intervals of each season are: interval 45
 428 (19 December) for winter, interval 11 (22 March) for spring, interval 23 (26 June) for
 429 summer and interval 34 (22 September) for autumn.
 430

431

Table 3. Number of observations for every RV (named as Interval).

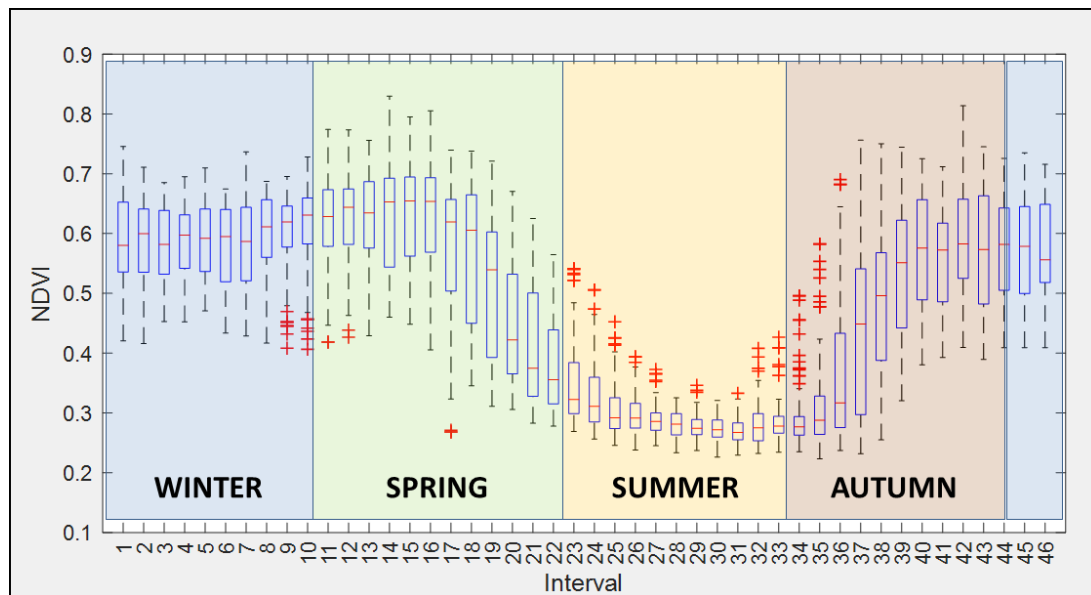
| RANDOM VARIABLE | # OBSERVATIONS | RANDOM VARIABLE | # OBSERVATIONS |
|------------------------|-----------------------|------------------------|-----------------------|
| Interval 1 | 85 | Interval 24 | 96 |
| Interval 2 | 84 | Interval 25 | 96 |
| Interval 3 | 96 | Interval 26 | 96 |
| Interval 4 | 96 | Interval 27 | 96 |
| Interval 5 | 95 | Interval 28 | 96 |
| Interval 6 | 90 | Interval 29 | 96 |
| Interval 7 | 86 | Interval 30 | 96 |
| Interval 8 | 83 | Interval 31 | 96 |
| Interval 9 | 96 | Interval 32 | 96 |
| Interval 10 | 96 | Interval 33 | 94 |
| Interval 11 | 74 | Interval 34 | 96 |
| Interval 12 | 88 | Interval 35 | 96 |
| Interval 13 | 88 | Interval 36 | 85 |
| Interval 14 | 88 | Interval 37 | 90 |
| Interval 15 | 96 | Interval 38 | 96 |
| Interval 16 | 92 | Interval 39 | 92 |
| Interval 17 | 88 | Interval 40 | 90 |
| Interval 18 | 96 | Interval 41 | 96 |
| Interval 19 | 95 | Interval 42 | 89 |
| Interval 20 | 96 | Interval 43 | 95 |
| Interval 21 | 95 | Interval 44 | 88 |
| Interval 22 | 96 | Interval 45 | 90 |
| Interval 23 | 96 | Interval 46 | 90 |

432

433

434 In Fig. 4, box plots of all RV with a start and end reference of the astronomical
 435 seasons are shown. The typical evolution of the NDVI along a year can be seen
 436 together with the inter-quartile range.

437



438

439

440

Figure 4. Box plots of 46 random variables (RV) are shown as well as start and end reference of every season. Study period from 2002 to 2017.

441

442

443

444

445

446

447

The observed evolution of NDVI through the different seasons is typical of the pasture in this area. The summer presents the lowest mean values which begin to increase in autumn achieving a maximum mean value of 0.60 or 0.65 during the beginning of spring. In the middle of the spring NDVI decrease again, approaching the lowest mean value of 0.28 approximately in summer.

448

449

450

451

452

Taking into account these values, dense vegetation, in this study pasture, is found from middle of October (interval 37) till the end of May (interval 19). It is in this period where the precipitation concentrates (see Table 1). During the summer, the NDVI mean values are lower than 0.3 corresponding with low precipitation and high temperatures.

453

454

455

456

457

458

459

460

Following the work of Escribano-Rodriguez et al. (2014), there is a relationship of pasture damage and a NDVI value around 0.40. Even if the authors point out that this value is highly variable depending on the location, we can see that summer season in this case study is under this value (see Fig. 4). This can explain that “Insurances for Damaged Pasture” usually do not apply in these dates due to the arid environment (BOE, 2013).

461

462

463

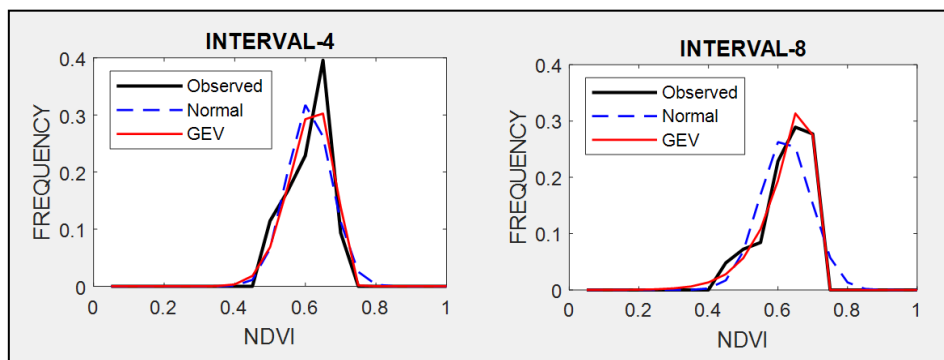
464

The statistical metric used in this study to assess the fit of the observed NDVI values with respect to the PDF candidates (Normal, Gamma, Beta and GEV) was the Chi square test (χ^2 test). The following steps were carried out:

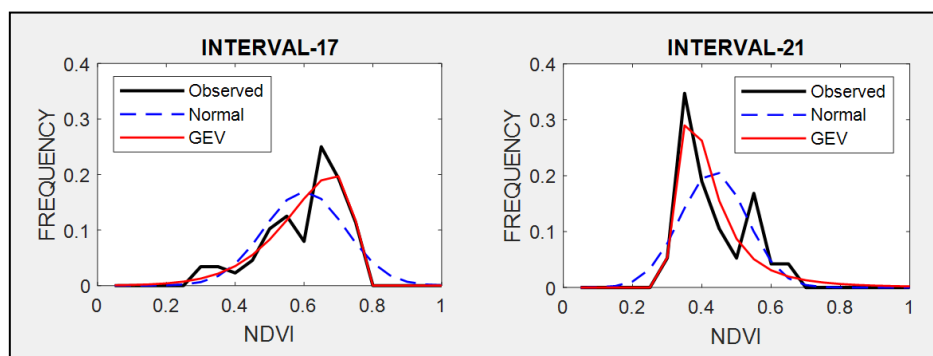
- 465 1. MLM was applied to model these 46 RV. Parameters were calculated for the
 466 four PDF candidates (see Table 2).
 467 2. To check the goodness of the fit of PDF candidates, a Chi square test (χ^2 test)
 468 was applied from 7 classes to 14 classes meeting the requirement that each
 469 class had at least five observations. The level of significance (α) was fixed to
 470 5% for all the candidates.
 471

472 3.2.1 Maximum Likelihood Method

473 Table A1 at Appendix A shows the estimated parameters for each PDF and each
 474 interval calculated by the MLM. These parameters were used to compare the
 475 estimated PDF with the NDVI observed values on different times through the seasons.
 476 The following intervals are shown as examples of better GEV fit: interval 4 and 8 (for
 477 winter, see Fig. 5), interval 17 and 21 (for spring, see Fig. 6) and interval 36 and 40 (for
 478 autumn, see Fig. 7). In these plots, observed frequency is compared versus Normal and
 479 GEV density distributions calculated by MLM.
 480

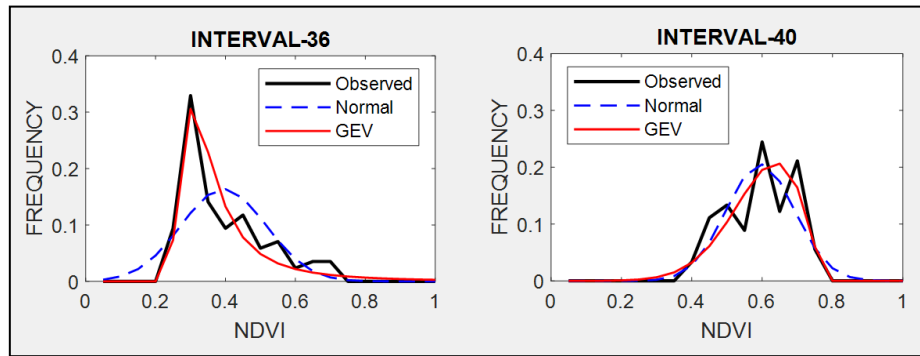


481
 482 **Figure 5.** Comparison between observed NDVI frequency, GEV and Normal probability density
 483 functions (PDF) on two different dates. Intervals 4 and 8 are examples for winter.



484
 485 **Figure 6.** Comparison between observed NDVI frequency, GEV and Normal probability density
 486 functions (PDF) on two different dates. Intervals 17 and 21 are examples for spring.

487



488

489

490

Figure 7. Comparison between observed NDVI frequency, GEV and Normal probability density functions (PDF) on two different times. Intervals 36 and 41 are examples for autumn.

491

492

493

494

495

496

497

498

499

500

501

During winter (see Fig. 5) the observed NDVI distribution presents negative skewness. Then, there is a higher frequency of high NDVI values corresponding with significant precipitation. During spring (see Fig. 6) an evolution in the skewness is observed passing from negative to positive, and so, the lower NDVI values become the higher probable. Finally, during autumn (see Fig. 7) precipitation begins and from positive pass to negative skewness and higher NDVI values are possible. We can observe that Normal distribution has no flexibility to follow this dynamic in the distributions on each time. This comparison is done in a sequential order for the whole of intervals in Figures A1, A2, A3 and A4 at Appendix A.

502

3.2.2 Chi square test

503

504

505

506

507

508

509

510

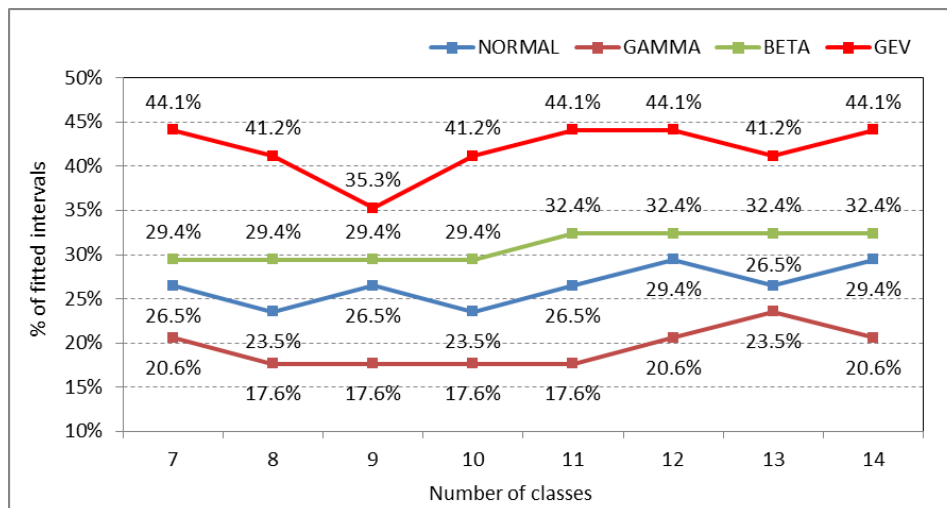
511

512

513

Twelve intervals (from 23 to 34) corresponding to the months of July, August and September have been excluded of this analysis since these intervals fall into the dry season in the study area, normally not covered by any SIBI. Therefore, calculations were carried out over 34 intervals.

To assess the general goodness of fit, the number of intervals where the χ^2 test was accepted (or failed to reject), were calculated for every PDF candidate. Then, the percentage of accepted intervals, over the total 34 intervals, was also calculated. Fig. 8 shows this percentage of intervals that fit for every PDF candidate. The number of classes used in χ^2 test is represented at the X-axis (from 7 to 14 classes).



514

515 **Figure 8.** Percentage of fitted intervals (Y axis) for each PDF candidate (Normal, Gamma, Beta
516 and GEV distributions) in function of the number of classes (X axis).

517

518 4. Discussion

519 4.1 Statistical context

520 Fig. 8 indicates that GEV distributions explain more intervals (more than 40% for
521 the majority of the class analysis) than the Normal, Gamma or Beta distributions. An
522 important difference between the Normal distribution and the PDFs used in this work
523 is their skewness and kurtosis. Many of the observed NDVI distributions present a clear
524 asymmetry and long tails in one or both sides that causes Normal distributions not to
525 be the optimal fit.

526

527 There is a relationship between seasons and the number of intervals that fit
528 correctly. We found that GEV distributions explain better intervals of spring and
529 autumn since their observed distributions are very asymmetric. On the other hand, we
530 did not find an important difference in winter, since the observed distributions are
531 mainly symmetric.

532

533 The more skewness and kurtosis depart from those of the Normal distribution the
534 larger the errors affecting the insurance designed based on Normal distributions
535 (Turvey et al., 2012). It is an expected result as pasture cultivation is quite different
536 from the development of arable crops, where Normal distributions in the NDVI values
537 are more common. This high heterogeneity in time and space of NDVI estimated on
538 pasture has been pointed out in several works (Martin-Sotoca et al, 2018). At the same
539 time, the more different the observed NDVI frequency is from a Normal distribution,
540 the less representative is the average, and so, the median becomes a more
541 representative value.

542

543 **4.2 Insurance context**

544 The use of NDVI thresholds in damaged pasture context was presented in the
 545 introduction section, being an example of using the "Insurance for Damaged Pasture"
 546 in Spain (BOE, 2013). We have chosen this last insurance to compare the results
 547 between applying Normal and GEV distribution methodologies. In this particular case
 548 the NDVI threshold ($NDVI_{th}$) was calculated using the expression $NDVI_{th} = \mu - k \cdot \sigma$
 549 (where μ, σ are average and standard deviation of NDVI distributions respectively,
 550 assuming the Normal hypothesis).

551

552 The probability of being below $NDVI_{th}$ (using $k = 0.7$, first damage level in the
 553 insurance) at every interval has been calculated assuming the Normal hypothesis. As it
 554 was expected, this value is always 24.2% (see third column in Table 4). The probability
 555 of being below $NDVI_{th}$ has also been calculated using GEV distributions obtained in
 556 this study. The probability obtained by GEV distributions is mostly lower than the
 557 Normal distributions in spring, autumn and winter (see Table 4) that is the working
 558 period of the insurance.

559

560 Observing where in time are the highest relative errors in probabilities (fifth
 561 column in Table 4), intervals corresponding to the end of winter, second middle of
 562 spring and the beginning of autumn present errors higher than 10%. This could explain
 563 why it is in spring and autumn when more disagreements exist between farmers and
 564 insurance company in claims.

565

566 **Table 4 – First column:** time intervals of approximately 8 days along the year. **Second column:**
 567 NDVI thresholds ($NDVI_{th}$) based on a Normal distribution applying $\mu - 0.7 \times \sigma$. **Third column:**
 568 percentages of area below the $NDVI_{th}$ when Normal distributions are applied. **Fourth column:**
 569 percentages of area below the $NDVI_{th}$ when GEV distributions are applied. **Fifth column:** relative
 570 area error of GEV compared to the Normal distribution.

571

| RANDOM VARIABLE | NORMAL | | GEV | |
|-----------------|-------------|--------|--------|-----------|
| | $NDVI_{th}$ | Prob. | Prob. | Error (%) |
| Interval 1 | 0.535 | 24.20% | 24.37% | 0.70% |
| Interval 2 | 0.541 | 24.20% | 23.18% | -4.21% |
| Interval 3 | 0.541 | 24.20% | 23.27% | -3.84% |
| Interval 4 | 0.543 | 24.20% | 23.27% | -3.84% |
| Interval 5 | 0.545 | 24.20% | 24.17% | -0.12% |
| Interval 6 | 0.534 | 24.20% | 21.48% | -11.24% |

| | | | | |
|-------------|-------|--------|--------|---------|
| Interval 7 | 0.528 | 24.20% | 24.01% | -0.79% |
| Interval 8 | 0.546 | 24.20% | 20.70% | -14.46% |
| Interval 9 | 0.555 | 24.20% | 21.30% | -11.98% |
| Interval 10 | 0.561 | 24.20% | 22.28% | -7.93% |
| Interval 11 | 0.567 | 24.20% | 23.49% | -2.93% |
| Interval 12 | 0.572 | 24.20% | 23.75% | -1.86% |
| Interval 13 | 0.571 | 24.20% | 23.20% | -4.13% |
| Interval 14 | 0.570 | 24.20% | 24.29% | 0.37% |
| Interval 15 | 0.571 | 24.20% | 23.47% | -3.02% |
| Interval 16 | 0.560 | 24.20% | 23.26% | -3.88% |
| Interval 17 | 0.495 | 24.20% | 21.29% | -12.02% |
| Interval 18 | 0.484 | 24.20% | 21.58% | -10.83% |
| Interval 19 | 0.442 | 24.20% | 23.06% | -4.71% |
| Interval 20 | 0.381 | 24.20% | 27.20% | 12.40% |
| Interval 21 | 0.342 | 24.20% | 29.46% | 21.74% |
| Interval 22 | 0.323 | 24.20% | 28.84% | 19.17% |
| Interval 35 | 0.257 | 24.20% | 18.98% | -21.57% |
| Interval 36 | 0.285 | 24.20% | 28.57% | 18.06% |
| Interval 37 | 0.333 | 24.20% | 25.90% | 7.02% |
| Interval 38 | 0.398 | 24.20% | 24.27% | 0.29% |
| Interval 39 | 0.454 | 24.20% | 23.79% | -1.69% |
| Interval 40 | 0.503 | 24.20% | 22.81% | -5.74% |
| Interval 41 | 0.491 | 24.20% | 23.23% | -4.01% |
| Interval 42 | 0.517 | 24.20% | 24.66% | 1.90% |
| Interval 43 | 0.507 | 24.20% | 23.13% | -4.42% |
| Interval 44 | 0.514 | 24.20% | 23.49% | -2.93% |
| Interval 45 | 0.515 | 24.20% | 23.70% | -2.07% |
| Interval 46 | 0.509 | 24.20% | 23.33% | -3.60% |

572

573 An alternative calculation can be the use of Normal probability (24.2%) to calculate
574 new $NDVI_{th}$ based on GEV (see Table 5). It can be seen that new $NDVI_{th}$ obtained
575 by GEV distributions are mostly higher than thresholds using Normal distributions in
576 spring, autumn and winter. Considering these results we find that damage thresholds
577 calculated by GEV distributions are mostly above the ones calculated by Normal
578 distributions.

579 Again, intervals corresponding to the end of winter, second middle of spring and the
580 beginning of autumn present $NDVI_{th}$ relative errors higher than 1% in absolute
581 values (fourth column in Table 5).

582

583 **Table 5 - First column:** time intervals of approximately 8 days along the year. **Second column:** NDVI
 584 thresholds ($NDVI_{Th}$) based on a Normal distribution (Normal) applying $\mu - 0.7 \times \sigma$. **Third column:**
 585 $NDVI_{Th}$ based on a GEV distribution (GEV) using 24.2% as the area below the $NDVI_{Th}$. **Fourth**
 586 **column:** relative $NDVI_{Th}$ error of GEV compared to the Normal distribution.

587

| RANDOM VARIABLE | NDVI _{Th} | | Error (%) |
|-----------------|--------------------|-------|-----------|
| | Normal | GEV | |
| Interval 1 | 0.535 | 0.534 | -0,19% |
| Interval 2 | 0.541 | 0.543 | 0,37% |
| Interval 3 | 0.541 | 0.543 | 0,37% |
| Interval 4 | 0.543 | 0.545 | 0,37% |
| Interval 5 | 0.545 | 0.545 | 0,00% |
| Interval 6 | 0.534 | 0.543 | 1,69% |
| Interval 7 | 0.528 | 0.528 | 0,00% |
| Interval 8 | 0.546 | 0.558 | 2,20% |
| Interval 9 | 0.555 | 0.563 | 1,44% |
| Interval 10 | 0.561 | 0.567 | 1,07% |
| Interval 11 | 0.567 | 0.569 | 0,35% |
| Interval 12 | 0.572 | 0.574 | 0,35% |
| Interval 13 | 0.571 | 0.574 | 0,53% |
| Interval 14 | 0.570 | 0.569 | -0,18% |
| Interval 15 | 0.571 | 0.573 | 0,35% |
| Interval 16 | 0.560 | 0.563 | 0,54% |
| Interval 17 | 0.495 | 0.510 | 3,03% |
| Interval 18 | 0.484 | 0.498 | 2,89% |
| Interval 19 | 0.442 | 0.447 | 1,13% |
| Interval 20 | 0.381 | 0.374 | -1,84% |
| Interval 21 | 0.342 | 0.334 | -2,34% |
| Interval 22 | 0.323 | 0.318 | -1,55% |
| Interval 35 | 0.257 | 0.262 | 1,95% |
| Interval 36 | 0.285 | 0.278 | -2,46% |
| Interval 37 | 0.333 | 0.327 | -1,80% |
| Interval 38 | 0.398 | 0.398 | 0,00% |
| Interval 39 | 0.454 | 0.455 | 0,22% |
| Interval 40 | 0.503 | 0.508 | 0,99% |
| Interval 41 | 0.491 | 0.494 | 0,61% |
| Interval 42 | 0.517 | 0.516 | -0,19% |
| Interval 43 | 0.507 | 0.510 | 0,59% |
| Interval 44 | 0.514 | 0.516 | 0,39% |
| Interval 45 | 0.515 | 0.516 | 0,19% |
| Interval 46 | 0.509 | 0.511 | 0,39% |

588

589

590 **5. Conclusions**

591 According to the results obtained in the study area using MLM and χ^2 test, it can
592 be concluded that Normal distributions are not a good fit to the NDVI observations,
593 and GEV distributions provide a better approximation.

594

595 The difference between Normal and GEV assumption is more evident in the
596 transition from winter to summer (spring), where NDVI values decrease, and then from
597 summer to winter (autumn) presenting the opposite behavior of increasing NDVI
598 values. In both periods asymmetrical distributions were found, negative skewness for
599 the spring transition and positive skewness for the autumn transition. During both
600 periods the variability in precipitation and temperatures were higher in this location.

601

602 We have found differences if GEV assumption is selected instead of the Normal
603 one when defining damaged pasture thresholds ($NDVI_{th}$). The use of these different
604 assumptions should be taken into account in future insurance implementations due to
605 the important consequences of supposing a damage event or not. We propose the use
606 of quantiles in observed NDVI distributions instead of average and standard deviation,
607 typically of Normal distributions, to calculate new $NDVI_{th}$.

608

609

610

611 **Acknowledgements**

612 This research has been partially supported by funding from MINECO under contract
613 No. MTM2015-63914-P and CICYT PCIN-2014-080.

614

615 **Appendix A**

616

617

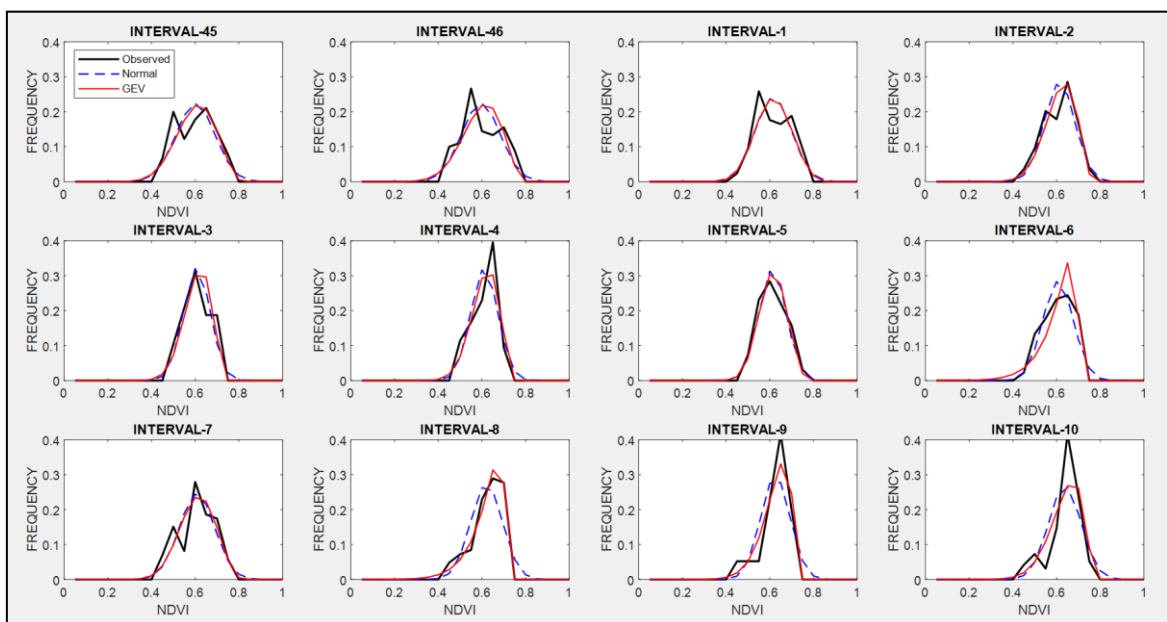
Table A1 - Maximum Likelihood parameters calculated for 4 PDF.

| RANDOM VARIABLE | NORMAL | | GAMMA | | BETA | | GEV | | |
|-----------------|--------|----------|----------|---------|--------|--------|-------|----------|--------|
| | μ | σ | α | β | a | b | μ | σ | ξ |
| Interval 1 | 0.591 | 0.081 | 53.31 | 0.011 | 21.45 | 14.82 | 0.563 | 0.080 | -0.297 |
| Interval 2 | 0.589 | 0.069 | 71.14 | 0.008 | 30.62 | 21.40 | 0.571 | 0.073 | -0.477 |
| Interval 3 | 0.583 | 0.060 | 94.15 | 0.006 | 39.56 | 28.34 | 0.567 | 0.063 | -0.457 |
| Interval 4 | 0.585 | 0.060 | 91.88 | 0.006 | 39.58 | 28.05 | 0.570 | 0.064 | -0.468 |
| Interval 5 | 0.588 | 0.061 | 93.92 | 0.006 | 38.83 | 27.25 | 0.568 | 0.061 | -0.340 |
| Interval 6 | 0.582 | 0.068 | 70.28 | 0.008 | 30.67 | 22.05 | 0.577 | 0.083 | -0.846 |
| Interval 7 | 0.584 | 0.080 | 52.52 | 0.011 | 22.16 | 15.82 | 0.559 | 0.082 | -0.366 |
| Interval 8 | 0.596 | 0.071 | 65.37 | 0.009 | 28.89 | 19.59 | 0.591 | 0.081 | -0.833 |
| Interval 9 | 0.601 | 0.066 | 76.02 | 0.008 | 34.31 | 22.84 | 0.590 | 0.070 | -0.652 |
| Interval 10 | 0.613 | 0.073 | 63.83 | 0.010 | 27.80 | 17.62 | 0.598 | 0.079 | -0.572 |
| Interval 11 | 0.621 | 0.078 | 58.72 | 0.011 | 24.33 | 14.86 | 0.600 | 0.083 | -0.451 |
| Interval 12 | 0.624 | 0.073 | 68.33 | 0.009 | 28.01 | 16.94 | 0.603 | 0.078 | -0.431 |
| Interval 13 | 0.624 | 0.075 | 66.22 | 0.009 | 26.23 | 15.85 | 0.604 | 0.080 | -0.476 |
| Interval 14 | 0.631 | 0.088 | 50.23 | 0.013 | 18.71 | 10.92 | 0.603 | 0.090 | -0.342 |
| Interval 15 | 0.630 | 0.084 | 53.60 | 0.012 | 21.17 | 12.45 | 0.607 | 0.089 | -0.448 |
| Interval 16 | 0.627 | 0.096 | 38.75 | 0.016 | 16.08 | 9.59 | 0.602 | 0.103 | -0.474 |
| Interval 17 | 0.577 | 0.117 | 20.47 | 0.028 | 10.24 | 7.58 | 0.560 | 0.127 | -0.692 |
| Interval 18 | 0.568 | 0.120 | 20.52 | 0.028 | 9.71 | 7.42 | 0.552 | 0.136 | -0.718 |
| Interval 19 | 0.523 | 0.116 | 19.46 | 0.027 | 9.52 | 8.68 | 0.495 | 0.125 | -0.493 |
| Interval 20 | 0.452 | 0.101 | 20.99 | 0.022 | 10.98 | 13.31 | 0.401 | 0.077 | 0.078 |
| Interval 21 | 0.409 | 0.095 | 19.94 | 0.021 | 11.18 | 16.13 | 0.354 | 0.060 | 0.325 |
| Interval 22 | 0.379 | 0.080 | 24.66 | 0.015 | 14.41 | 23.52 | 0.333 | 0.046 | 0.385 |
| Interval 23 | 0.353 | 0.073 | 26.54 | 0.013 | 15.85 | 29.01 | 0.311 | 0.036 | 0.456 |
| Interval 24 | 0.328 | 0.056 | 38.36 | 0.009 | 24.22 | 49.65 | 0.298 | 0.033 | 0.287 |
| Interval 25 | 0.305 | 0.044 | 53.52 | 0.006 | 35.62 | 81.20 | 0.282 | 0.028 | 0.210 |
| Interval 26 | 0.298 | 0.034 | 78.93 | 0.004 | 54.47 | 128.55 | 0.283 | 0.029 | -0.064 |
| Interval 27 | 0.289 | 0.026 | 126.85 | 0.002 | 88.33 | 217.15 | 0.278 | 0.021 | -0.030 |
| Interval 28 | 0.282 | 0.022 | 166.17 | 0.002 | 119.50 | 305.03 | 0.274 | 0.022 | -0.322 |
| Interval 29 | 0.278 | 0.021 | 179.09 | 0.002 | 127.93 | 332.63 | 0.269 | 0.018 | -0.085 |
| Interval 30 | 0.273 | 0.019 | 203.11 | 0.001 | 147.67 | 393.21 | 0.266 | 0.019 | -0.247 |
| Interval 31 | 0.272 | 0.022 | 166.83 | 0.002 | 120.11 | 321.95 | 0.262 | 0.018 | -0.059 |
| Interval 32 | 0.280 | 0.034 | 75.63 | 0.004 | 52.36 | 134.30 | 0.264 | 0.023 | 0.118 |
| Interval 33 | 0.285 | 0.034 | 82.05 | 0.004 | 54.90 | 137.68 | 0.270 | 0.020 | 0.122 |
| Interval 34 | 0.295 | 0.057 | 33.26 | 0.009 | 21.15 | 50.37 | 0.268 | 0.024 | 0.363 |
| Interval 35 | 0.312 | 0.079 | 19.70 | 0.016 | 11.83 | 25.94 | 0.275 | 0.038 | 0.300 |
| Interval 36 | 0.369 | 0.121 | 10.81 | 0.034 | 6.11 | 10.33 | 0.298 | 0.063 | 0.480 |
| Interval 37 | 0.432 | 0.141 | 9.45 | 0.046 | 5.21 | 6.81 | 0.370 | 0.120 | -0.080 |

| | | | | | | | | | |
|--------------------|-------|-------|-------|-------|-------|-------|-------|-------|--------|
| Interval 38 | 0.487 | 0.128 | 13.88 | 0.035 | 7.25 | 7.63 | 0.445 | 0.127 | -0.321 |
| Interval 39 | 0.529 | 0.107 | 23.56 | 0.022 | 11.39 | 10.16 | 0.497 | 0.110 | -0.390 |
| Interval 40 | 0.570 | 0.096 | 34.02 | 0.017 | 15.10 | 11.40 | 0.548 | 0.105 | -0.533 |
| Interval 41 | 0.554 | 0.090 | 36.42 | 0.015 | 16.90 | 13.64 | 0.531 | 0.096 | -0.471 |
| Interval 42 | 0.583 | 0.095 | 37.29 | 0.016 | 15.56 | 11.11 | 0.551 | 0.094 | -0.295 |
| Interval 43 | 0.574 | 0.097 | 34.27 | 0.017 | 14.93 | 11.07 | 0.550 | 0.103 | -0.482 |
| Interval 44 | 0.572 | 0.083 | 47.13 | 0.012 | 20.40 | 15.26 | 0.549 | 0.086 | -0.425 |
| Interval 45 | 0.576 | 0.088 | 42.59 | 0.014 | 18.17 | 13.36 | 0.550 | 0.090 | -0.396 |
| Interval 46 | 0.570 | 0.088 | 41.98 | 0.014 | 18.11 | 13.66 | 0.546 | 0.092 | -0.445 |

618

619



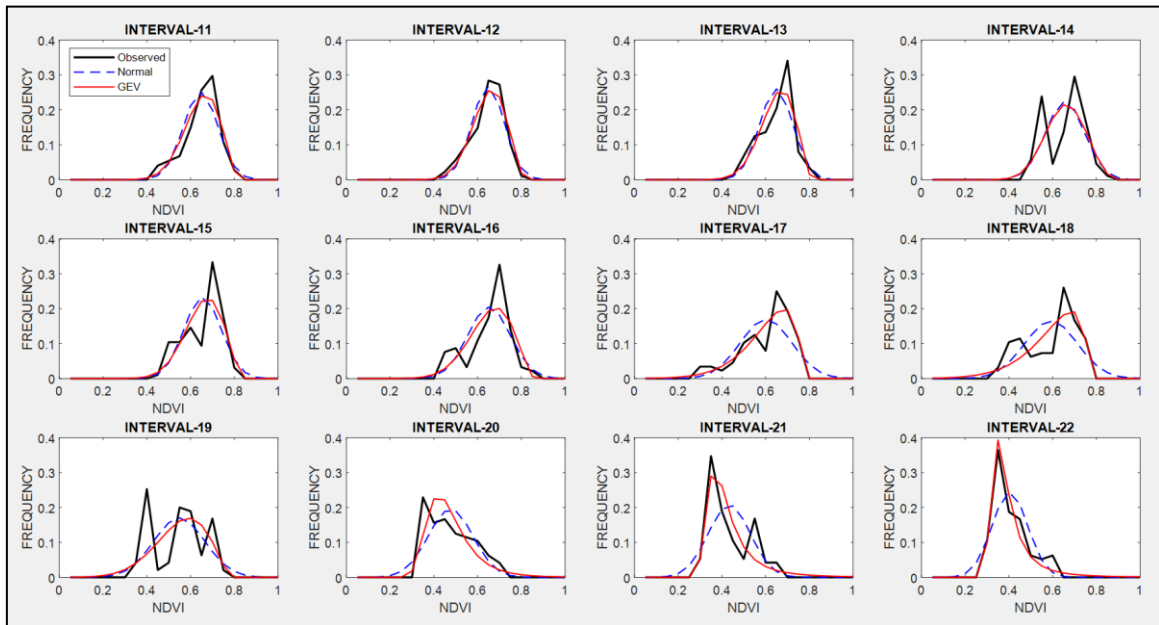
620

621

622

Figure A1. Observed NDVI, GEV and Normal probability density functions (PDF) from interval 45 to interval 10 (from 19 December to 21 March) representing winter.

623



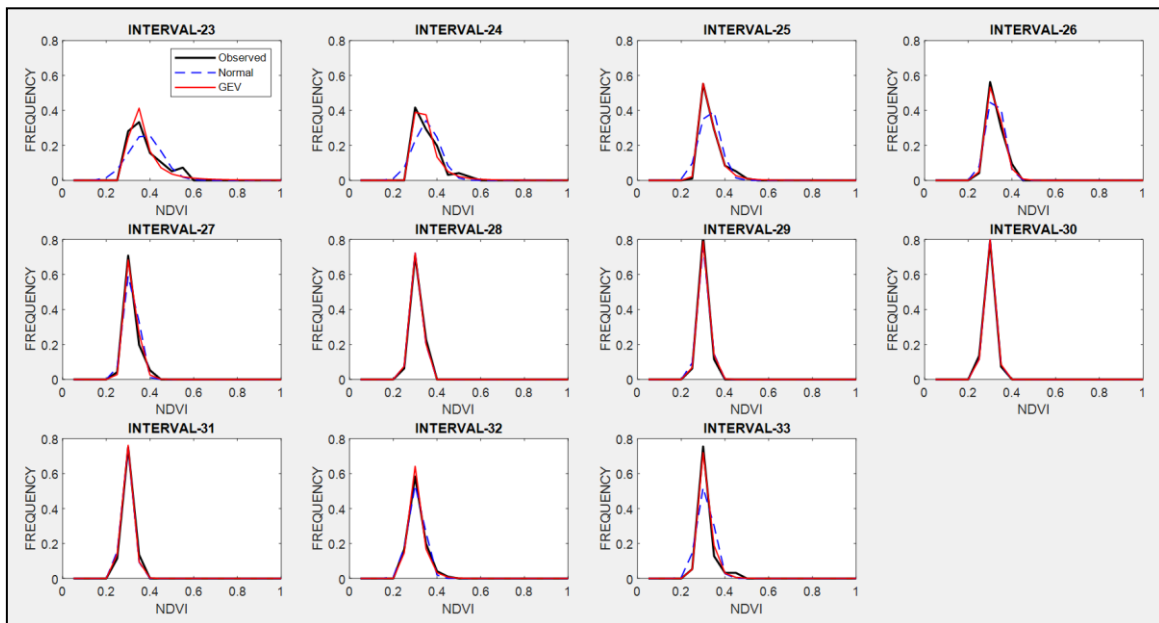
624

625

626

Figure A2. Observed NDVI, GEV and Normal probability density functions (PDF) from interval 11 to interval 22 (from 22 March to 25 June) representing spring.

627



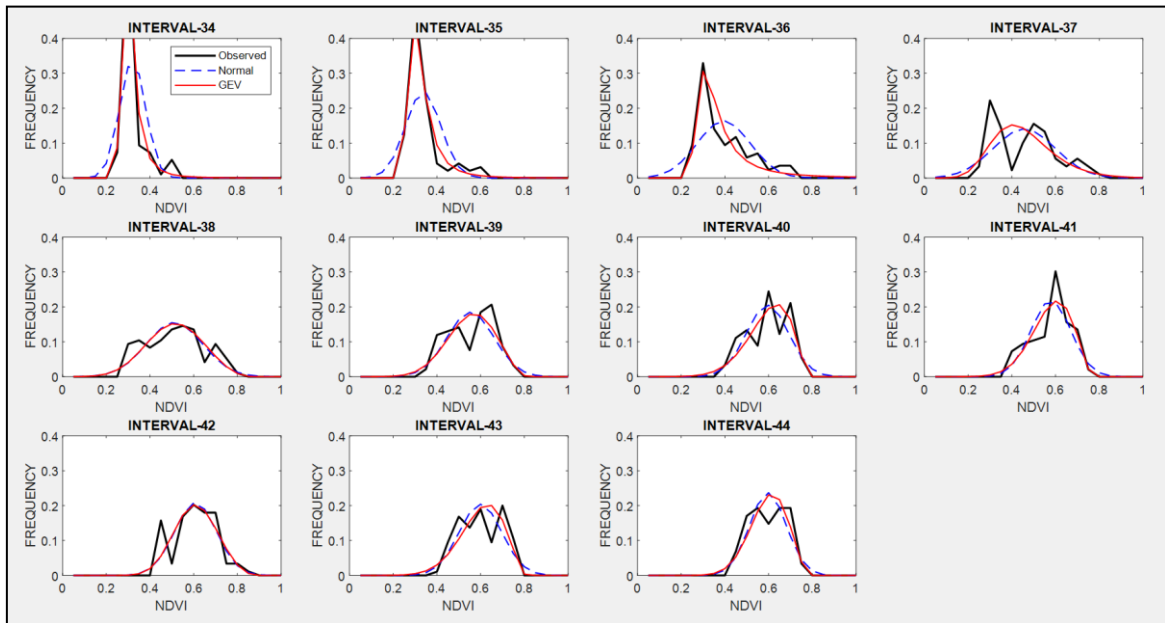
628

629

630

Figure A3. Observed NDVI, GEV and Normal probability density functions (PDFs) from interval 23 to interval 33 (from 26 June to 21 September) representing summer.

631



632

633

634

Figure A4. Observed NDVI, GEV and Normal PDFs from interval 34 to interval 44 (from 22 September to 18 December) representing autumn.

635

636 **References**

637

638 Agencia Estatal de Meteorología (AEMET). Available at: www.aemet.es, 2017.639 Al-Bakri, J. T., and Taylor, J. C.: Application of NOAA AVHRR for monitoring vegetation
640 conditions and biomass in Jordan, *J. Arid Environ*, 54, 579–593, 2003.641 Anyamba, A., and Tucker, C.J.: Historical perspective of AVHRR NDVI and vegetation
642 drought monitoring. In: *Remote Sensing of Drought: Innovative Monit Approaches*,
643 pp. 23, 2012.644 Bailey, S.: *The Impact of Cash Transfers on Food Consumption in Humanitarian Settings:*
645 *A review of evidence, Study for the Canadian Foodgrains Bank, May 2013.*646 Bayarjargal, Y., Karnieli, A., Bayasgalan, M., Khudulmur, S., Gandush, C., and Tucker,
647 C.J.: A comparative study of NOAA-AVHRR derived drought indices using change
648 vector analysis, *Remote Sens. Environ.* 105 (1), 9–22, 2006.649 Boletín Oficial del Estado (BOE, 6638 - Orden AAA/1129/2013. Nº 145, III, p-46077,
650 2013.651 Cochran, William G.: The Chi-square Test of Goodness of Fit, *Annals of Mathematical*
652 *Statistics.* 23: 315–345, 1952.653 Crimmins, M. A., and Crimmins T. M.: Monitoring plant phenology using digital repeat
654 photography, *Environ. Manage*, 41, 949-958, 2008.655 Dalezios, N. R., Blanta, A., Spyropoulos, N. V., and Tarquis A. M.: Risk identification of
656 agricultural drought for sustainable Agroecosystems, *Nat. Hazards Earth Syst. Sci.*,
657 14, 2435–2448, 2014.658 Dalezios, N. R.: The Role of Remotely Sensed Vegetation Indices in Contemporary
659 Agrometeorology. Invited paper in Honorary Special Volume in memory of late
660 Prof. A. Flokas. Publisher: Hellenic Meteorological Association, 33-44, 2013.661 De Leeuw, J., Vrieling, A., Shee, A., Atzberger, C., Hadgu, K. M., Biradar, C. M.,
662 Humphrey Keah, H., and Turvey, C.: The Potential and Uptake of Remote Sensing in
663 Insurance: A Review, *Remote Sens.*, 6(11), 10888-10912, 2014.664 Escribano Rodríguez, J. Agustín, Díaz-Ambrona, Carlos Gregorio H., and Tarquis Alfonso,
665 Ana María: Selection of vegetation indices to estimate pasture production in
666 Dehesas, *PASTOS*, 44(2), 6-18, 2014.667 Fensholt, R., and Proud, S. R.: Evaluation of earth observation based global long term
668 vegetation trends - comparing GIMMS and MODIS global NDVI time series, *Remote*
669 *Sens. Environ.*, 119, 131–147, 2012.670 Flynn E. S.: Using NDVI as a pasture management tool. Master Thesis, University of
671 Kentucky, 2006.672 Forkel, M., Carvalhais, N., Verbesselt, J., Mahecha, M.D., Neigh, C. S., and Reichstein,
673 M.: Trend change detection in NDVI time series: effects of inter-annual variability
674 and methodology, *Remote Sens.*, 5, pp, 2113–2144, 2013.675 Fuller, D.O.: Trends in NDVI time series and their relation to rangeland and crop
676 production in Senegal, 1987–1993, *Int. J. Remote Sens.*, 19, 2013–2018, 1998.

- 677 Gommès, R., and Kayitakire, F.: The challenges of index-based insurance for food
678 security in developing countries. Proceedings, Technical Workshop, JRC, Ispra, 2-3
679 May 2012. Publisher: JRC-EC, p. 276, 2013.
- 680 Gouveia, C., Trigo, R. M., and Da Camara, C. C.: Drought and vegetation stress
681 monitoring in Portugal using satellite data, *Nat. Hazards Earth Syst. Sci.*, 9, 185-195,
682 2009.
- 683 Goward, S. N., Tucker, C. J., and Dye, D.G.: North-American vegetation patterns
684 observed with the NOAA-7 advanced very high-resolution radiometer. *Vegetation*,
685 64, 3–14, 1985.
- 686 Graham, E. A., Yuen, E. M., Robertson, G. F., Kaiser, W. J., Hamilton, M. P., and Rundel,
687 P. W.: Budburst and leaf area expansion measured with a novel mobile camera
688 system and simple color thresholding, *Environ. Exp. Bot.*, 65, 238-244, 2009.
- 689 Hobbs, T. J.: The use of NOAA-AVHRR NDVI data to assess herbage production in the
690 arid rangelands of central Australia, *Int. J. Remote Sens.*, 16, 1289–1302, 1995.
- 691 Holben, B. N.: Characteristics of maximum-value composite images from temporal
692 AVHRR data, *Int. J. Remote Sens.*, 7, 1417–1434, 1986.
- 693 Kottek, M., Grieser, J., Beck, C., Rudolf, B., and Rubel, F.: World Map of the
694 Köppen-Geiger climate classification updated, *Meteorologische Zeitschrift*, 15,
695 259-263, 2006.
- 696 Kundu, A., Dwivedi, S., and Dutta, D.: Monitoring the vegetation health over India
697 during contrasting monsoon years using satellite remote sensing indices, *Arab J*
698 *Geosci.*, 9, 144, 2016.
- 699 Land Processes Distributed Active Archive Center (LP DAAC): Surface Reflectance 8-Day
700 L3 Global 500m. NASA and USGS. Available at:
701 https://lpdaac.usgs.gov/products/modis_products_Table/mod09a1. 2014.
- 702 Larson, H. J.: Introduction to Probability Theory and Statistical Inference (3rd edition).
703 New York, John Wiley and Sons, 1982.
- 704 Leblois, A.: Weather index-based insurance in a cash crop regulated sector: ex ante
705 evaluation for cotton producers in Cameroon. Paper presented at the JRC/IRI
706 workshop on The Challenges of Index-Based Insurance for Food Security in
707 Developing Countries, Ispra, 2-3, May, 2012.
- 708 Lovejoy, S., Tarquis, A. M., Gaonac’h, H., and Schertzer, D.: Single and Multiscale
709 remote sensing techniques, multifractals and MODIS derived vegetation and soil
710 moisture. *Vadose Zone J.*, 7, 533-546, 2008.
- 711 Li, R., Tsunekawa, A., and Tsubo, M.: Index-based assessment of agricultural drought in
712 a semi-arid region of Inner Mongolia, China, *J. Arid Land* 6 (1), 3–15, 2014.
- 713 Maples, J. G., Brorsen, B. W., and Biermaches, J. T.: The rainfall Index Annual Forage
714 pilot program as a risk management tool for cool-season forage. *J. Agr. Appl Econ*,
715 48(1), 29–51, 2016.
- 716 Martin-Sotoca, J. J., Saa-Requejo, A., Orondo J. B., and Tarquis, A. M.: Singularity maps
717 applied to a vegetation index, *Bio. Eng.* 168, 42-53, 2018.

- 718 Motohka, T., Nasahara, K. N., Murakami, K., and Nagai, S.: Evaluation of sub-pixel cloud
719 noises on MODIS daily spectral indices based on in situ measurements, *Remote*
720 *Sens.*, 3, 1644–1662, 2011.
- 721 Nanzad, L., Zhang, J., Tuvdendorj, B., Nabil, M., Zhang, S., and Bai, Y.: NDVI anomaly for
722 drought monitoring and its correlation with climate factors over Mongolia from
723 2000 to 2016, *Journal of Arid Environments* Volume 164, Pages 69-77, 2019.
- 724 Niemeyer, S.: New drought indices, First Int. Conf. on Drought Management: Scientific
725 and Technological Innovations, Zaragoza, Spain. Joint Research Centre of the
726 European Commission, Available online at
727 <http://www.iamz.ciheam.org/medroplan/zaragoza2008/Sequia2008/Session3/S.Niemeyer.pdf>, 2008.
728
- 729 Ortega-Farias, S., Ortega-Salazar, S., Poblete, T., Kilic, A., Allen, R., Poblete-Echeverría,
730 C., Ahumada-Orellana, L., Zuñiga, M., and Sepúlveda, D.: Estimation of Energy
731 Balance Components over a Drip-Irrigated Olive Orchard Using Thermal and
732 Multispectral Cameras Placed on a Helicopter-Based Unmanned Aerial Vehicle
733 (UAV), *Remote Sens.*, 8, 638, pp 18, 2016.
- 734 Park, S.: Cloud and cloud shadow effects on the MODIS vegetation index composites of
735 the Korean Peninsula, *Int. J. Remote Sens.*, 34, 1234–1247, 2013.
- 736 Peters, A. J., E. A. Walter-Shea, L. Ji, A. Vina, M. Hayes, and M.D. Svoboda: Drought
737 monitoring with NDVI-Based Standardized Vegetation Index, *Photogrammetric*
738 *Engineering and Remote Sensing* 68:71–75, 2002.
- 739 Rao, K. N.: Index based Crop Insurance, *Agric. Agric. Sci. Proc.*, 1, 193–203, 2010.
- 740 Roumigué, A., Sigel, G., Poilvé, H., Bouchard, B., Vrieling, A., and Jacquin, A.: Insuring
741 forage through satellites: testing alternative indices against grassland production
742 estimates for France, *Int. J. Remote Sens.*, 38, 1912-1939, 2017.
- 743 Roumigué, A., Jacquin, A., Sigel, G., Poilvé, H., Lepoivre, B., and Hagolle, O.:
744 Development of an index-based insurance product: validation of a forage
745 production index derived from medium spatial resolution fCover time series,
746 *GIScience Remote Sens.*, 52, 94-113, 2015.
- 747 Tackenberg, Oliver: A New Method for Non-destructive Measurement of Biomass,
748 Growth Rates, Vertical Biomass Distribution and Dry Matter Content Based on
749 Digital Image Analysis, *Annals of Botany*, 99(4), 777–783, 2007.
- 750 Turvey, C. G., and McAurin, M. K.: Applicability of the Normalized Difference Vegetation
751 Index (NDVI) in Index-Based Crop Insurance Design, *Am. Meteorol. Soc.*, 4, 271-284,
752 2012.
- 753 UNEP Word Atlas of Desertification: Second Ed. United Nations Environment Programme,
754 Nairobi, 1997.
- 755 USDA. U.S. Department of Agriculture, Federal Crop Insurance Corporation, Risk
756 Management Agency: Rainfall Index Plan Annual Forage Crop Provisions. 16- RI-AF.
757 <http://www.rma.usda.gov/policies/ri-vi/2015/16riaaf.pdf> 2013 (Accessed March 1,
758 2018).

759 Wei, W., Wu, W., Li, Z., Yang, P., and Qingbo Zhou, Q.: Selecting the Optimal NDVI
760 Time-Series Reconstruction Technique for Crop Phenology Detection, *Intell. Autom.*
761 *Soft. Co.* 22, 237-247, 2016.
762
763
764